7-21-2020

Analysis of Temperature-Dependent H/D Exchange Mass Spectrometry Experiments.

Nastaran N Tajoddin

Lars Konermann

Analysis of Temperature-Dependent H/D Exchange Mass Spectrometry Experiments

Nastaran N. Tajoddin and Lars Konermann*

Department of Chemistry, The University of Western Ontario, London, Ontario, N6A 5B7, Canada

* To whom correspondence should be addressed. E-mail: konerman@uwo.ca.

Funding was provided by the Natural Sciences and Engineering Research Council of Canada (RGPIN-2018-04243).

Abstract: H/D exchange (HDX) mass spectrometry (MS) is a widely used technique for interrogating protein structure and dynamics. Backbone HDX is mediated by opening/closing (unfolding/refolding) fluctuations. In traditional HDX-MS, proteins are incubated in D_2O as a function of time at constant temperature (T). There is an urgent need to complement this traditional approach with experiments that probe proteins in a T-dependent fashion, e.g., for assessing the stability of therapeutic antibodies. A key problem with such studies is the absence of strategies for interpreting HDX/MS data in the context of T-dependent protein dynamics. Specifically, it has not been possible thus far to separate T-induced changes of the chemical labeling step (k_{ch}) from thermally enhanced protein fluctuations. Focusing on myoglobin, the current work solves this problem by dissecting T-dependent HDX-MS profiles into contributions from $k_{ch}(T)$, as well as local and global protein dynamics. Experimental profiles started off with surprisingly shallow slopes that seemed to defy the quasi-exponential $k_{ch}(T)$ dependence. Just below the melting temperature (T_m) the profiles showed a sharp increase. Our analysis revealed that local dynamics dominate at low T, while global events become prevalent closer to T_m. About half of the backbone NH sites exhibited a canonical scenario, where local opening/closing was associated with positive ΔH and ΔS. Many of the remaining sites had negative ΔH and ΔS, thereby accounting for the shallowness of the experimental HDX-MS profiles at low T. In summary, this work provides practitioners with the tools to analyze proteins over a wide temperature range, paving the way toward T-dependent high-throughput screening applications by HDX-MS.

Native proteins undergo incessant thermal motions, from local fluctuations to global unfolding/refolding.[1, 2] These dynamics reflect the fact proteins continuously explore their conformational space. The population of each conformer depends on its free energy,[2] while interconversion rates are governed by activation barriers.[3] Protein dynamics are linked to biological function such as catalysis,[4] energy conversion,[5] and signaling.[6] However, protein fluctuations can also generate structures that act as gateway to cytotoxic aggregates.[7, 8]

Hydrogen/deuterium exchange (HDX) mass spectrometry (MS) is one of the most widely used tools for interrogating protein dynamics.[5, 8-15] HDX-MS complements other techniques such as Förster resonance energy transfer, time-resolved X-ray diffraction, and NMR spin relaxation studies.[16] HDX-MS monitors the deuteration of backbone NH groups upon exposure to D_2O. In native proteins most of these sites are engaged in NH···OC hydrogen bonds. According to the widely accepted Linderstrøm-Lang model (eq. 1)[2, 17] native state HDX is mediated by opening/closing (unfolding/refolding) fluctuations that transiently disrupt H-bonds.

$$NH_{closed} \underset{k_{cl}}{\overset{k_{op}}{\rightleftarrows}} NH_{open} \xrightarrow[D_2O]{k_{ch}} exchanged \qquad (1)$$

Here, k_{op} and k_{cl} are the opening and closing rate constants, and k_{ch} is the "chemical" rate constant.[18] HDX usually proceeds in the EX2 limit ($k_{cl} >> k_{ch}$),[2] where each NH undergoes many opening/closing transition before it is deuterated. The overall HDX rate constant in this case is

$$k_{HDX} = K_{op} \times k_{ch} \qquad (2)$$

where $K_{op} = k_{op}/k_{cl}$. Hence, HDX kinetics are governed by NH_{open} sites, even though the population of these sites tends to be very low (typically << 1%).[2, 19, 20] Dynamic regions (larger K_{op}) exhibit faster HDX, while labeling of rigid segments (smaller K_{op}) proceeds more slowly.

In conventional HDX-MS a protein is incubated in D_2O at constant temperature. Aliquots sampled at various time points are subjected to proteolysis, followed by LC/MS to uncover the deuteration percentage (%*D*) of individual peptides. In addition to these conventional measurements, there is growing interest in temperature-dependent HDX-MS. The latter can provide a more comprehensive view of protein dynamics.[21-29] Of particular importance is the characterization of thermally stressed protein drugs (such as therapeutic antibodies) to assess their stability and aggregation propensity.[15, 30, 31]

It is well known that elevated temperatures tend to enhance HDX,[21-29] but the origins of this effect are non-trivial. Temperature controls HDX via two avenues. (1) The labeling chemistry (k_{ch} in eq. 1) accelerates quasi-exponentially with temperature[18] due to a combination of Arrhenius behavior and changes in the concentration of OD^- catalyst.[32, 33] (2) Temperature governs the Boltzmann populations of NH_{open} states,[2] and it alters the protein energy landscape.[34] HDX-MS aims to uncover protein behavior (contribution 2), but unfortunately this aspect tends to be masked by temperature-dependent changes of k_{ch} (contribution 1). Preliminary steps have been taken to unravel this problem,[20, 25, 35-37] but a comprehensive strategy for analyzing HDX-MS data as a function of temperature (T) and time (t) is still lacking. The current work fills this void by deconvoluting experimental HDX-MS data into the two aforementioned contributions.

Protein stability studies usually rely on a two-state approximation involving the native state N and the unfolded state U.[34] The free energy of the global N $\leftrightarrow$ U equilibrium is

$$\Delta G_{glob} = \Delta H_{glob} - T\,\Delta S_{glob} \qquad (3)$$

N is stable as long as $\Delta G_{glob} > 0$. Simple analyses often assume that enthalpy ($\Delta H_{glob} > 0$) and entropy ($\Delta S_{glob} > 0$) are constant, such that ΔG_{glob} depends linearly on T.[38] Heating causes ΔG_{glob} to turn negative at the melting temperature T_m, thereby triggering unfolding. A more thorough

treatment of eq. 3 has to consider ΔC_p, the heat capacity difference between U and N which causes ΔH_{glob} and ΔS_{glob} to become T-dependent ($\Delta C_p > 0$)[34]

$$\Delta H_{glob}(T) = \Delta H_{glob}(T_m) + \Delta C_p \times (T - T_m) \quad (4a)$$

$$\Delta S_{glob}(T) = \Delta S_{glob}(T_m) + \Delta C_p \times \ln(T/ T_m) \quad (4b)$$

where $\Delta S_{glob}(T_m) = \Delta H_{glob}(T_m)/T_m$.[38] Eq. 4 implies that $\Delta G_{glob}(T)$ is curved. As a result, proteins are most stable at an intermediate temperature. Raising the temperature beyond T_m triggers heat-induced unfolding. Cooling causes destabilization as well; depending on the magnitude of ΔC_p this can cause cold-unfolding (see Figure S1 for a summary of these concepts).[39-41]

Eqs. 3 and 4 are key pillars of protein thermodynamics.[34, 38] However, it is undisputed that two-state N $\leftrightarrow$ U models do not fully capture the protein behavior, especially at ambient T where local fluctuations dominate over global unfolding/refolding.[1, 2] For addressing this deficiency and for interpreting T-dependent HDX-MS data it is necessary to combine the Linderstrøm-Lang model (eqs. 1, 2)[2, 17] with the thermodynamic principles expressed in eqs. 3, 4.

Building on the aforementioned ideas, the current work devises a strategy for analyzing T-dependent HDX-MS data. Like many previous studies on protein thermodynamics,[39] folding,[42] fluctuations,[1] and aggregation,[43] we chose the heme protein myoglobin (Mb) as model system. Mb has a globular native structure, where a hydrophobic core is surrounded by solvent-exposed polar and charged residues.[44] We tracked the HDX response of Mb to changes in T, and we captured the resulting data using a comprehensive T- and t-dependent HDX data analysis framework.

Methods

Materials. Horse-heart ferri-Mb (Sigma, St. Louis, MO) samples were centrifuged to remove small amounts of insoluble debris. All solutions contained 50 mM sodium phosphate buffer and 100 mM NaCl at a pH meter reading adjusted to 7.2 (corresponding to pD 7.6 for D_2O-based solutions).[18, 45] This value was *T*-independent with deviations of less than ± 0.1, consistent with previous reports on the temperature stability of phosphate buffer.[46]

H/D Exchange Mass Spectrometry. HDX was performed by adding 50 μM Mb solution in H_2O buffer to D_2O labeling buffer in a 1:9 ratio, for a final protein concentration of 5 μM in 90% D_2O. All measurements were performed with careful temperature control, by placing the samples in Eppendorf tubes that were immersed in a water bath during labeling. An ice/water mix was used for measurements at 0 °C, while HDX between 23 °C and 80 °C was performed by employing a heated circulating bath. Prior to initiating HDX, D_2O labeling buffer was pre-equilibrated at the desired temperature, while Mb was kept at 23 °C to avoid aggregation in the stock solution. Two types of HDX experiments were performed. (i) [variable *T*, constant *t*] was conducted by using a deuteration time of *t* = 30 s. (ii) For [constant *T*, variable *t*] aliquots were removed at *t* = 30 s, 10 min, and 100 min. HDX was quenched by mixing with HCl, resulting in a pH meter reading of 2.4. This was followed by flash freezing and storage in $N_2(l)$. For analysis, the samples were rapidly thawed and injected into an Acquity HDX-UPLC (Waters, Milford, MA). Digestion was performed on an immobilized pepsin column (Thermo Fisher) at 15 °C. Peptides were separated on a 1.7 μm BEH130 C18 2.1 mm × 100 mm column using a 20 min water/acetonitrile gradient in the presence of 0.1% formic acid at ~0 °C. The sequence coverage was 98% (Figure S2). Blanks were injected to prevent carryover. In addition, the pepsin column was washed with 1.5 M

guanidine hydrochloride in water/acetonitrile/formic acid (95.2/4/0.8) after each digestion step. The UPLC was coupled to a Waters Synapt G2 mass spectrometer with a lock spray dual electrospray source. The identity of each peptide was confirmed by MS^E on non-deuterated samples with data analysis by Waters PLGS 2.5.3, based on the known Mb sequence (pdb 1wla[44]). The capillary voltage and desolvation temperature were +2.8 kV and 250 °C respectively. The centroid mass of each peptide isotope distribution was calculated using DynamX 3.0 (Waters) and converted to percent deuteration (*%D*) according to $\%D = [(m - m_0)/(m_{100} - m_0)] \times 100\%$, where m is the centroid *m/z* for the peptide of interest. m_0 and m_{100} correspond to minimally and fully deuterated controls, respectively. The former were prepared by adding Mb to pre-quenched D_2O buffer, followed by flash freezing. m_{100} samples were prepared similar to m_0 samples, except that they were incubated for 3 days at 37 °C. Back-exchange levels determined from m_{100} samples were (38 ± 14)%, similar to previous reports.[35, 47] All %*D* values are averages of three independent replicates; error bars represent standard deviations. Circular dichroism (CD) measurements were performed as outlined in the SI.

Elevated temperatures may cause protein aggregation[48] which would complicate the interpretation of HDX and CD experiments. Aggregation can be suppressed by working with dilute solutions.[42, 49] For the experiments of this work we therefore used a relatively low Mb concentration (5 μM), where aggregation was negligible for at least 20 min even when heated to 358 K (85 °C). This assertion is based on aggregation assays on Mb that had been heated for different *t* and *T*, followed by centrifugation and UV-Vis analyses of the supernatant.

Results and Discussion

Spectroscopic Characterization of Global Unfolding. Heat-induced unfolding of Mb was probed by CD spectroscopy. Spectra acquired at different T intersected at ~204 nm (Figure 1A). This isodichroic point is consistent with a global N $\leftrightarrow$ U transition,[39, 50] justifying the application of eqs. 3 and 4. Thermal unfolding profiles were recorded by monitoring CD_{222} at different heating rates (1 °C min^{-1} and 4 °C min^{-1}) in both H_2O and in D_2O. All of the resulting CD_{222} profiles were very similar, with T_m = 356.2 ± 0.6 K and $\Delta H_{glob}(T_m)$ = 453 ± 20 kJ mol^{-1} (Figure 1B).

As is common practice in optical melting experiments,[38] the aforementioned analysis assumed that $\Delta C_p = 0$, such that ΔG_{glob} depends linearly on temperature (Figure 1C, dotted line, eq. 3). Alternatively, one can perform an analysis with ΔC_p = 8 kJ mol^{-1} K^{-1}, a value determined by differential scanning calorimetry (DSC).[39, 51] This ΔC_p value with the T_m and $\Delta H_{glob}(T_m)$ noted above corresponds to a curved ΔG_{glob} profile (Figure 1C, solid line, eq. 4). Both ΔG_{glob} profiles match the experimental data equally well (Figure 1B), but the curved profile in Figure 1C is more realistic because it takes into account the DSC-derived ΔC_p value.[39, 51] This curved ΔG_{glob} profile will serve as starting point for the analysis of T-dependent HDX-MS data.

Temperature- and Time-Dependent HDX Experiments. Figures S3A and S3B exemplify peptide isotope distributions acquired after exposing Mb to D_2O for different times at T = 296 K (23 °C). With increasing t the spectra shifted to higher m/z because of backbone deuteration. A complementary perspective was obtained by conducting HDX in a T-dependent fashion between 273 K and 353 K, while keeping the labeling time t constant. We chose t = 30 s, which resulted in a wide dynamic range of $\%D$ values. Mass spectra measured in this way demonstrate that

increased *T* dramatically enhances the extent of deuteration (Figure S3C). In fact, the *T*-induced spectral changes were much larger than those seen in the *t*-dependent data of Figure S3A and S3B.

T-dependent *%D* profiles revealed interesting differences for the various Mb regions (Figure 2). Many of the profiles showed very shallow slopes between 273 K and ~340 K, e.g., 30-40 and 111-126. These shallow slopes are surprising, considering that k_{ch} increases quasi-exponentially with *T*.[18] Several profiles had an upwards kink at 348 K. This feature is most pronounced for 111-126, but it also affects 12-20, 21-29, 30-40, 56-69, 87-106, and 124-134. The SI Appendix summarizes all *T*- and *t*-dependent data, including peptides not shown in Figure 2.

Developing a Temperature-Dependent HDX-MS Model. We now examine how *T*-dependent changes in labeling chemistry and protein dynamics manifest themselves in the HDX behavior, ultimately yielding a model that accounts for all the experimental data (solid line fits in Figure 2A and in the SI Appendix). The deuteration behavior of a peptide with *N* non-proline residues covering amino acids *k* to (*k*+*N*-1) can be described as[52-54]

$$\%D(T,t) = \frac{1}{(N-2)}\sum_{i=(k+2)}^{N}[\,1 - \exp\left(-k_{HDX,i}(T)\ \times t\right)] \qquad (5)$$

where $k_{HDX,i}(T)$ is the HDX rate constant of NH *i*. Summation starts at *k*+2 because the first two residues undergo complete back exchange during LC.[18, 35, 55] Layer by layer, the following sections describe a strategy to capture the behavior of $k_{HDX,i}(T)$ in eq. 5 (Figure 3). We were guided by the tenets that a good model will (i) be able to quantitatively match the experimental data, (ii) be as simple as possible, and (iii) have a minimum number of adjustable parameters.

Layer 1: Temperature Dependence of k_{ch}. Before focusing on protein dynamics we examine the chemical rate constant k_{ch} that governs the deuteration of NH_{open} (eq. 1). k_{ch} depends on T, pD, and neighboring side chains.[18, 56] Its T-dependence is often described using the Arrhenius expression[18]

$$k_{ch}(T) = k_{ch_{298}} \times \exp\left(-\frac{Ea_{eff}}{R}(T^{-1} - [298\ K]^{-1})\right) \quad (6a)$$

where k_{ch_298} is a reference value for 298 K, and the effective activation energy E_{a_eff} is 71.1 kJ mol^{-1} (Figures S4, S5).[56] However, eq. 6a is only an approximation.[18] The actual E_a for chemical exchange is 12.6 kJ mol^{-1}.[18] The T-dependence of k_{ch} arises largely from changes in [OD$^-$] as governed by the T-dependent ionization constant K_{D2O} = [D$^+$][OD$^-$],[32] keeping in mind that HDX in near-neutral solution is OD$^-$ catalyzed.[33] The analyses below use the more accurate expression

$$k_{ch}(T) = k_{B\_298} \times \exp\left(-\frac{E_a}{R}(T^{-1} - [298\ K]^{-1})\right) \times [OD^-](T) \quad (6b)$$

with the reference value k_{B_298} for base-catalyzed exchange (Figure S5).[18] Between 0 °C and ~60 °C the $k_{ch}(T)$ profiles predicted by eqs. 6a and 6b are similar. At 80 °C the eq. 6a value is 34% larger than that of eq. 6b; at higher T the differences become more pronounced (Figure S5).

Layer 2: Verifying the EX2 Regime. The interpretation of HDX-MS data requires different approaches, depending on whether deuteration proceeds in the EX1 or in the EX2 regime.[5, 8-15] EX2, defined as $k_{cl} >> k_{ch}$ (eq. 1), represents the most common scenario; it is associated with unimodal isotope distribution that gradually shift to higher mass.[2, 12, 19, 20] EX1 ($k_{cl} << k_{ch}$) is less common. Cooperative EX1 dynamics cause bimodal isotope distributions.[12, 19, 20] The unimodal nature of the spectra in this work confirms that HDX proceeds in the EX2 regime (Figure S3). Skeptics might bring up an interesting issue in this context. Because k_{ch} increases with T,[18] heating might cause a transition from EX2 ($k_{cl} >> k_{ch}$) at low T to EX1 ($k_{cl} << k_{ch}$) at high T. However,

such an EX2 → EX1 transition is unlikely, because k_{cl} and k_{ch} *both* increase with T (Figure S6). We conclude that eq. 2, which represents the central paradigm of the EX2 regime, represents a reasonable foundation for analyzing the HDX behavior of Mb.

Individual NH sites exhibit single-exponential EX2 kinetics only if the NH_{open} population in eq. 1 is small ($k_{cl} >> k_{op}$).[2, 17] To ensure that this criterion is being met, our analysis will not consider data beyond 353 K (80 °C) where the population of U reaches ~22% (Figure S1). In the next few paragraphs will use two peptides, 1-7 and 21-29, to illustrate the remaining layers of the model (Figure 3).

Layer 3: Protein Dynamics at High Temperature (Close to 353 K). There is some uncertainty regarding the exact nature of the opening/closing fluctuations in eq. 1.[57, 58] As a starting point we try to equate these fluctuations with global N ↔ U transitions such that eq. 2 turns into

$$k_{HDX,i}(T) = \exp[\, -\Delta G_{glob}(T)/RT\,] \times k_{ch,i}(T) \qquad (7a)$$

where $\Delta G_{glob}(T)$ is the free energy derived from CD melting data (Figure 1C). Figure 3A-D compares the predictions of eq. 7a with experimental $\%D(T, 30\text{ s})$ data for peptides 1-7 and 21-29. We ignore, for now, the mismatch at low T and focus on higher temperatures. For peptide 1-7 the eq. 7a prediction agrees well with experiments for $T \geq 338$ K, where $\%D$ approaches 100% (Figure 3A). In contrast, peptide 21-29 shows major discrepancies at high T, with experimental $\%D$ values that are much lower than predicted by eq. 7a (dotted line in Figure 3C).

The high-temperature mismatch in Figure 3C implies that the unfolded state in the CD-detected N ↔ U equilibrium retains some HDX protection for peptide 21-29. This interpretation is consistent with reports of residual structure in many other unfolded proteins,[59, 60] which causes NH sites to exchange slower than in dipeptides.[55, 56, 61] In other words, HDX for peptide 21-29 must

involve a two-step opening process ($N \leftrightarrow U_{cl} \leftrightarrow U_{op}$), where the first step corresponds to the CD-detected $\Delta G_{glob}(T)$. In the context of eq. 1, U_{cl} represents a "closed" (exchange-incompetent) state. The subsequent $U_{cl} \leftrightarrow U_{op}$ transition generates the HDX-competent "open" state, and this opening event is associated with an additional free energy ΔG_{opU}. Overall, the $N \leftrightarrow U_{op}$ equilibrium thus has a free energy of

$$\Delta G^*_{glob}(T) = \Delta G_{glob}(T) + \Delta G_{opU} \qquad (7b)$$

(Figure 3D). For peptide 21-29, ΔG_{opU} = 22 kJ mol^{-1} generates a HDX profile that agrees quite well with the experimental data above 348 K (solid in Figure 3C). In summary, we account for residual protection of heat-unfolded Mb by modifying eq. 7a according to

$$k_{HDX,i}(T) = \exp[\, -\Delta G^*_{glob}(T)/RT\,] \times k_{ch,i}(T) \qquad (7c)$$

where $\Delta G^*_{glob}(T)$ is defined in eq. 7b and $\Delta G_{opU} \geq 0$ represents a fitting parameter. U segments without residual protection have ΔG_{opU} = 0 (such as 1-7, Figure 3B). In principle, ΔG_{opU} will depend on T as expressed in eq. 4. However, ΔG_{opU} makes its presence felt only in a narrow range close to T_m, such that the ΔH and ΔS components of ΔG_{opU} cannot be determined. To avoid the use of such ill-defined parameters, we will therefore assume that ΔG_{opU} is T-independent.

Layer 4: Local Fluctuations. The Layer 3 considerations refer to relatively high temperatures (around 353 K) where global unfolding/refolding starts to make its presence felt.[34] At lower T global dynamics are less prevalent, and HDX occurs mainly via local fluctuations.[2, 58] Englander et al.[2] suggested that the interplay of local and global dynamics can be captured by replacing K_{op} in eq. 2 with the sum K_{op}(local) + K_{op}(global). We build on this idea by expanding eq. 2 according to

$$k_{HDX,i}(T) = [\, K_{op\_loc}(T) + K^*_{op\_glob}(T) \,] \times k_{ch,i}(T) \qquad (8)$$

The equilibrium constant K_{op_loc} in eq. 8 describes local opening/closing fluctuations which are associated with the free energy $\Delta G_{loc}(T)$, such that $K_{op\_loc} = \exp[\, -\Delta G_{loc}(T)/RT \,]$ with $\Delta G_{loc}(T) = \Delta H_{loc} - T\Delta S_{loc}$. To avoid "overfitting", we make the approximation that these local events have $\Delta C_p = 0$. As discussed in Layer 3, $K^*_{op\_glob} = \exp[\, -\Delta G^*_{glob}(T)/RT \,]$ describes the $N \leftrightarrow U_{op}$ equilibrium. Eq. 8 expresses the idea[2] that any NH site can reach an open state via two types of dynamics, such that k_{HDX} is the sum of both kinetic channels. When putting it all together, eq. 8 turns into

$$k_{HDX,i}(T) = (\, \exp[\, -(\Delta H_{loc} - T\Delta S_{loc})/RT \,] + \exp[\, -(\Delta G_{glob}(T) + \Delta G_{opU})/RT \,] \,) \times k_{ch,i}(T) \qquad (9)$$

Fitting of the adjustable parameters (ΔG_{opU}, ΔH_{loc}, and ΔS_{loc}) results in greatly improved agreement with the experimental $\%D(T, 30\text{ s})$ profiles for both test peptides (Figure 3E and H). Here we assumed that all NH sites in any given peptide share the same thermodynamic parameters, a limitation that will be improved upon in the following section.

Layer 5: Inclusion of time-Dependent Data. For extending our model to labeling times beyond $t = 30$ s we included data at $t = 600$ s and 6000 s at 296 K and 333 K. These temperatures were chosen because they provided $\%D(T, t)$ values that covered a wide dynamic range. The inclusion of these additional time points provides much more stringent constraints for the model parameters.

Layer 4 provides a poor description of the HDX data for $t > 30$ s (Figure 3G, J). Luckily, a minor modification is sufficient to remedy this mismatch. So far we assumed that all NH sites in a peptide share the same ΔG_{opU}, ΔH_{loc}, ΔS_{loc}. We now eliminate this unrealistic restriction. In principle each NH site should have its own ΔG_{opU}, ΔH_{loc}, and ΔS_{loc}. However, such an approach would imply an unrealistically large number of fitting parameters (~148 × 3 = 444), generating a

mathematically underdetermined situation. To avoid this problem we chose a compromise where each peptide was divided into segments. NH sites in each segment share the same ΔG_{opU}, ΔH_{loc}, ΔS_{loc}. This segmentation concept is borrowed from the widely accepted foldon model,[2] where groups of adjacent NH sites open/close with the same thermodynamic parameters. In Figure 3 we dissected peptides into two segments, e.g., peptide 1-7 was divided into segments 3-4 and 5-7. Residues 1-2 were not considered because of back exchange.[18, 35, 55] After this modification, eq. 9 provided excellent agreement with the experimental data for all *T* and *t* (Figures 3K/N and O/R).

Layer 6: Global Fitting. Many Mb regions were covered by overlapping peptides. Rather than fit each peptide individually (as in Layer 5), this overlap allows the implementation of a global fitting strategy (Note: this term refers to a data analysis method;[53, 54, 62-64] it is unrelated to "global" unfolding). Segments that are shared across multiple peptides were modeled using the same ΔG_{opU}, ΔH_{loc}, ΔS_{loc}. Global fitting improves the robustness and accuracy of results compared to single-curve analyses, and it reduces the number of parameters (see SI for details).[53, 54, 62-64] The 22 peptides with the highest S/N were subjected to global fitting (Figure S7) by minimizing

$$X^2 = \sum_{peptides} \sum_T \sum_t (\%D_{exp} - \%D_{calc})^2 \qquad (10)$$

where the summation includes multiple peptides, *T*, and *t* values. $\%D_{exp}$ refers to experimental data. $\%D_{calc}$ values were calculated using eq. 9. Preliminary segment boundaries were first determined by analyzing one peptide at a time. If treating a peptide as a single segment did not yield an acceptable fit, it was divided into two, then three segments, etc. For global fitting these preliminary boundaries had to be slightly adjusted to ensure consistency across overlapping peptides. In the end, Mb was dissected into 44 segments, each of which had its own ΔG_{opU}, ΔH_{loc}, ΔS_{loc} (44 × 3 = 132 parameters, segment boundaries are denoted as vertical lines in Figure S7).

Applying the Model to Experimental HDX Data. HDX-MS data for Mb acquired as a function of T and t were analyzed using eq. 9. Gratifyingly, our model produced excellent fits for all 22 peptides, illustrated in Figure 2A for selected $\%D(T, 30\ s)$ profiles. The complete data set is shown in the SI Appendix. Fitted ΔG_{opU}, ΔH_{loc}, ΔS_{loc} parameters are compiled in Figure 4.

ΔG_{opU} Values. Consistent with previous observations,[55, 56, 59-61] our data show that the CD-detected globally unfolded state retains residual protection. Deuteration of U_{cl} is mediated by opening/closing transitions with a free energy ΔG_{opU}. Most of the fitted ΔG_{opU} values fell in the range of 20 to 40 kJ mol^{-1} (Figure 4A). The similarity of ΔG_{opU} across much of the protein could suggest the occurrence of cooperative $U_{cl} \leftrightarrow U_{op}$ fluctuations.[2] However, the presence of independently fluctuating segments cannot be ruled out.

ΔH_{loc} and ΔS_{loc} Values. Before examining the remaining fitting parameters we note that N ↔ U equilibria can follow different thermodynamic scenarios. (i) Unfolding is often endothermic ($\Delta H > 0$) because energy is required to dissociate contacts within the protein that stabilize N (e.g., H-bonds). Under these conditions the enhanced conformational freedom of U usually results in $\Delta S > 0$.[38, 39] In the context of global Mb unfolding this scenario applies for $T > 303$ K, where the slope of $\Delta G_{glob}(T)$ is negative (Figure 3B). (ii) N ↔ U equilibria can also be exothermic ($\Delta H < 0$) with $\Delta S < 0$,[39, 65] as seen in Figure 3B for $T < 303$ K where $\Delta G_{glob}(T)$ has a positive slope. The origin of this second scenario remains poorly understood,[41] but the assembly of tightly H-bonded shell water around unfolded regions likely plays a role.[66] Figures S1C and S1D illustrate both scenarios, highlighting that there is also an intermediate regime where both ΔH and ΔS are close to zero.

The aforementioned two scenarios are well established for *global* N ↔ U equilibria.[39, 65, 66] It is reasonable to assume that these concepts also extend to *local* closed ↔ open fluctuations. Consistent with this expectation, our HDX fits yielded positive as well as negative ΔH_{loc} and ΔS_{loc} values (Figure 4B, C). Segments with $\Delta H_{loc} > 0$ and $\Delta S_{loc} > 0$ were located mostly within long helices (such as B, G, and H), corresponding to scenario (i) described above. Conversely, most segments with $\Delta H_{loc} < 0$ and $\Delta S_{loc} < 0$ (scenario ii) were found at helix/loop boundaries (Figure 4B, C). This spatial distribution is intriguing, but from the data presented here it cannot be decided why these specific regions follow one scenario versus the other.

Interplay of Local and Global Dynamics. It is gratifying that eq. 9 can capture the entire HDX-MS data set for different T and t (Figure 2A, SI Appendix). We will illustrate the underlying T-dependent local and global dynamics for two residues, L32 and G124 (Figure 5); these were selected because of their particularly large $|\Delta H_{loc}|$ and $|\Delta S_{loc}|$ (asterisks in Figure 4B, C).

The HDX behavior of any NH site is governed by the opening/closing fluctuation with the lowest ΔG (the largest K_{op}).[2] Accordingly, HDX of L32 is dominated by local fluctuations throughout the entire T range, while global events are negligible (Figure 5A, B). As expressed in eq. 8, multiplication of the K_{op} "Sum" (red line in Figure 5B) with k_{ch} (Figure 5C) yields k_{HDX} (Figure 5D). The resulting $\%D(T)$ profile increases toward 100% in a near-exponential fashion (Figure 5E). This steep $\%D(T)$ rise results from three effects: 1. k_{HDX} increases with T (Figure 5D). 2. The $\exp(-T^{-1})$ dependence in eq. 9 favors open conformations at high T. 3. $\Delta G_{loc}(T)$ has a negative slope ($\Delta S_{loc} > 0$) which further promotes the open state at high T (Figure 5A).

The experimental $\%D(T, 30\text{ s})$ profiles of many Mb peptides had very shallows slopes at low T, followed by a sudden increase close to T_m (e.g. peptide 111-126 in Figure 2A). It would be

impossible to model these data if all NH sites had rapidly increasing *%D* profiles similar to that of Figure 5E. A look at G124 reveals how our model solves this problem. G124 has $\Delta S_{loc} < 0$, resulting in a positive slope for ΔG_{loc} that suppresses local opening with increasing T. At 343 K the ΔG_{loc} and ΔG^*_{glob} curves intersect; beyond this temperature HDX takes place mainly via global dynamics (Figure 5F). As a result, $k_{HDX}(T)$ decreases slightly between 273 K and 343 K, followed by a sudden upward kink (Figure 5I). This behavior is echoed in the $\%D(T, 30\ s)$ profile of Figure 5J as well as the experimental data of peptide 111-126 (Figure 2A).

In summary, Mb dynamics at low T are dominated by local fluctuations. For some of these local fluctuations $\Delta G_{loc}(T)$ decreases, while for others $\Delta G_{loc}(T)$ increases with T. The latter account for the very shallow slopes that were experimentally observed for many $\%D(T)$ profiles at low T. The conspicuous kink of the experimental $\%D(T)$ data at around 343 K results from a crossover of $\Delta G_{loc}(T)$ and $\Delta G_{glob}(T)$, marking the point at which global fluctuations start to dominate.

Conclusions

For the first time, the current work provides a thermodynamic model that can quantitatively describe temperature-dependent protein HDX-MS data. For conventional time-dependent HDX-MS experiments it is common to use multi-exponential fits with apparent rate constants (see SI for more details).[52] Unfortunately, that conventional approach only yields a phenomenological description of the data, and the fitting parameters obtained are difficult to interpret in a structural/thermodynamic context. This is in contrast to the temperature-dependent model developed here, where the fitting parameters directly report on first-principle protein properties (ΔG_{opU}, ΔH_{loc}, and ΔS_{loc}).

The analysis strategy presented here captures the interplay of local fluctuations (which dominate at low T) and global unfolding/refolding (which becomes prevalent closer to T_m). Some of the local fluctuations are associated with $\Delta H_{loc} > 0$ and $\Delta S_{loc} > 0$, representing the canonical scenario[38, 39] where thermal energy is required to disrupt local noncovalent contacts, and where locally unfolded segments are more disordered than in the native state. On the other hand, there are also local events with $\Delta H_{loc} < 0$ and $\Delta S_{loc} < 0$. The structural origin of this second scenario remains to be fully elucidated, but it may be caused by tightly H-bonded water around the locally unfolded regions.[39, 65, 66] The second scenario is indispensable for modeling the shallow slopes seen for many of the experimental HDX profiles at low temperature. Another essential ingredient of our model is residual HDX protection of the globally unfolded state, implying that U undergoes transient opening transitions that are associated with ΔG_{opU}. This phenomenon is consistent with studies on many other proteins.[55, 56, 59-61]

This work provides practitioners with a tool for analyzing HDX-MS data across a wide range of temperatures, e.g., for assessing the thermal stability of protein therapeutics.[15, 30, 31] The key steps required for applying this method are as follows: (i) Ensure that the protein does not aggregate in the T range of interest. (ii) Determine global unfolding parameters (T_m, $\Delta H_{glob}(T_m)$, ΔC_p) by CD spectroscopy, DSC, or from the literature. (iii) Measure $\%D$ for overlapping peptides over a wide temperature range and at different time points, and verify EX2 behavior. (iv) Perform global fitting on the basis of eq. 9.

An interesting aspect of temperature-dependent HDX-MS is the dramatically shortened time scale. Traditional room temperature assays routinely employ labeling times up to many hours,[5, 8-15] whereas the current work demonstrates that complete HDX profiles can be generated in as little as 30 s (Figure 2A). With robotic technology it should be possible to develop temperature-

dependent HDX-MS workflows for high-throughput applications such as excipient screening[30] or drug candidate binding tests.[11] In any case, it is hoped that the current work will encourage practitioners to explore the use of temperature-dependent HDX-MS, instead of being confined to traditional time-domain measurements.

Supporting Information. SI Text: Additional Methods Details (CD Spectroscopy); Discussion of Global Fitting Strategy. Supporting Figures: Thermodynamics of protein unfolding. Peptic digestion map. Time- and temperature dependent HDX mass spectra. $k_{ch,i}$ values for Mb. *T*-dependence of k_{ch}. Transition state theory applied to opening/closing dynamics. Segment assignment for global fitting. Temperature-dependent ΔG profiles. SI Appendix: Complete HDX data set with fits.

References

(1) Frauenfelder, H.; Chen, G.; Berendzen, J.; Fenimore, P. W.; Jansson, H.; McMahon, B. H.; Stroe, I. R.; Swenson, J.; Young, R. D. A unified model of protein dynamics. *Proc. Natl. Acad. Sci. U.S.A.* **2009**, 106, 5129-5134.

(2) Bai, Y.; Sosnick, T. R.; Mayne, L.; Englander, S. W. Protein Folding Intermediates: Native State Hydrogen Exchange. *Science* **1995**, 269, 192-197.

(3) Neupane, K.; Foster, D. A. N.; Dee, D. R.; Yu, H.; Wang, F.; Woodside, M. T. Direct observation of transition paths during the folding of proteins and nucleic acids. *Science* **2016**, 352, 239-242.

(4) Hanoian, P.; Liu, C. T.; Hammes-Schiffer, S.; Benkovic, S. Perspectives on Electrostatics and Conformational Motions in Enzyme Catalysis. *Accounts Chem. Res.* **2015**, 48, 482-489.

(5) Murcia Rios, A.; Vahidi, S.; Dunn, S. D.; Konermann, L. Evidence for a Partially Stalled γ Rotor in F1-ATPase from Hydrogen–Deuterium Exchange Experiments and Molecular Dynamics Simulations. *J. Am. Chem. Soc.* **2018**, 140, 14860-14869.

(6) Boehr, D. D.; Nussinov, R.; Wright, P. E. The role of dynamic conformational ensembles in biomolecular recognition. *Nat. Chem. Biol.* **2009**, 5, 789-796.

(7) Balchin, D.; Hayer-Hartl, M.; Hartl, F. U. In vivo aspects of protein folding and quality control. *Science* **2016**, 353, 42.

(8) Rob, T.; Liuni, P.; Gill, P. K.; Zhu, S. L.; Balachandran, N.; Berti, P. J.; Wilson, D. J. Measuring Dynamics in Weakly Structured Regions of Proteins Using Microfluidics-Enabled Subsecond H/D Exchange Mass Spectrometry. *Anal. Chem.* **2012**, 84, 3771-3779.

(9) Pirrone, G. F.; Iacob, R. E.; Engen, J. R. Applications of Hydrogen/Deuterium Exchange MS from 2012 to 2014. *Anal. Chem.* **2015**, 87, 99-118.

(10) Rand, K. D.; Zehl, M.; Jorgensen, T. J. D. Measuring the Hydrogen/Deuterium Exchange of Proteins at High Spatial Resolution by Mass Spectrometry: Overcoming Gas-Phase Hydrogen/Deuterium Scrambling. *Acc. Chem. Res.* **2014**, 47, 3018-3027.

(11) Marciano, D. P.; Dharmarajan, V.; Griffin, P. R. HDX-MS guided drug discovery: small molecules and biopharmaceuticals. *Curr. Op. Struct. Biol.* **2014**, 28, 105-111.

(12) Percy, A. J.; Rey, M.; Burns, K. M.; Schriemer, D. C. Probing protein interactions with hydrogen/deuterium exchange and mass spectrometry-A review. *Anal. Chim. Acta* **2012**, 721, 7-21.

(13) Martens, C.; Shekhar, M.; Lau, A. M.; Tajkhorshid, E.; Politis, A. Integrating hydrogen deuterium exchange mass spectrometry with molecular dynamics simulations to probe lipid-modulated conformational changes in membrane proteins. *Nat. Protoc.* **2019**, 14, 3183-3204.

(14) Habibi, Y.; Uggowitzer, K. A.; Issak, H.; Thibodeaux, C. J. Insights into the Dynamic Structural Properties of a Lanthipeptide Synthetase using Hydrogen-Deuterium Exchange Mass Spectrometry. *J. Am. Chem. Soc.* **2019**, 141, 14661-14672.

(15) Masson, G. R.; Jenkins, M. L.; Burke, J. E. An overview of hydrogen deuterium exchange mass spectrometry (HDX-MS) in drug discovery. *Expert. Opin. Drug Discov.* **2017**, 12, 981-994.

(16) van den Bedem, H.; Fraser, J. S. Integrative, dynamic structural biology at atomic resolution-it's about time. *Nat. Methods* **2015**, 12, 307-318.

(17) Hvidt, A.; Nielsen, S. O. Hydrogen exchange in proteins. *Adv. Protein Chem.* **1966**, 21, 287-386.

(18) Bai, Y.; Milne, J. S.; Mayne, L.; Englander, S. W. Primary Structure Effects on Peptide Group Hydrogen Exchange. *Proteins: Struct., Funct., Genet.* **1993**, 17, 75-86.
(19) Konermann, L.; Pan, J.; Liu, Y. Hydrogen Exchange Mass Spectrometry for Studying Protein Structure and Dynamics. *Chem. Soc. Rev.* **2011**, 40, 1224-1234.
(20) Xiao, H.; Hoerner, J. K.; Eyles, S. J.; Dobo, A.; Voigtman, E.; Mel'Cuk, A. I.; Kaltashov, I. A. Mapping protein energy landscapes with amide hydrogen exchange and mass spectrometry: I. A generalized model for a two-state protein and comparison with experiment. *Protein Sci.* **2005**, 14, 543-557.
(21) Xiao, P.; Bolton, D.; Munro, R. A.; Brown, L. S.; Ladizhansky, V. Solid-state NMR spectroscopy based atomistic view of a membrane protein unfolding pathway. *Nat. Commun.* **2019**, 10.
(22) van de Waterbeemd, M.; Llauro, A.; Snijder, J.; Valbuena, A.; Rodriguez-Huete, A.; Fuertes, M. A.; de Pablo, P. J.; Mateu, M. G.; Heck, A. J. R. Structural Analysis of a Temperature-Induced Transition in a Viral Capsid Probed by HDX-MS. *Biophys. J.* **2017**, 112, 1157-1165.
(23) Lim, X. X.; Chandramohan, A.; Lim, X. Y. E.; Crowe, J. E.; Lok, S. M.; Anand, G. S. Epitope and Paratope Mapping Reveals Temperature-Dependent Alterations in the Dengue-Antibody Interface. *Structure* **2017**, 25, 1391-1402.
(24) Offenbacher, A. R.; Hu, S. S.; Poss, E. M.; Carr, C. A. M.; Scouras, A. D.; Prigozhin, D. M.; Iavarone, A. T.; Palla, A.; Alber, T.; Fraser, J. S.; Klinman, J. P. Hydrogen-Deuterium Exchange of Lipoxygenase Uncovers a Relationship between Distal, Solvent Exposed Protein Motions and the Thermal Activation Barrier for Catalytic Proton-Coupled Electron Tunneling. *ACS Central Sci.* **2017**, 3, 570-579.
(25) Liang, Z.-X.; Lee, T.; Resing, K. A.; Ahn, N. G.; Klinman, J. P. Thermal-activated protein mobility and its correlation with catalysis in thermophilic alcohol dehydrogenase. *Proc. Natl. Acad. Sci. U.S.A.* **2004**, 101, 9556-9561.
(26) Banks, D. D.; Zhang, J.; Siska, C. C. Relationship between Native-State Solubility and Non-Native Aggregation of Recombinant Human Granulocyte Colony Stimulating Factor: Practical Implications for Protein Therapeutic Development. *Mol. Pharm.* **2014**, 11, 3431-3442.
(27) Man, P.; Fabry, M.; Sieglova, I.; Kavan, D.; Novak, P.; Hnizda, A. Thiopurine intolerance-causing mutations in NUDT15 induce temperature-dependent destabilization of the catalytic site. *BBA-Proteins Proteomics* **2019**, 1867, 376-381.
(28) Rist, W.; Jorgensen, T. J. D.; Roepstorff, P.; Bukau, B.; Mayer, M. P. Mapping temperature-induced conformational changes in the Escherichia coli heat shock transcription factor sigma(32) by amide hydrogen exchange. *J. Biol. Chem.* **2003**, 278, 51415-51421.
(29) Cirri, E.; Brier, S.; Assal, R.; Canul-Tec, J. C.; Chamot-Rooke, J.; Reyes, N. Consensus designs and thermal stability determinants of a human glutamate transporter. *Elife* **2018**, 7.
(30) Toth, R. T.; Pace, S. E.; Mills, B. J.; Joshi, S. B.; Esfandiary, R.; Middaugh, C. R.; Weis, D. D.; Volkin, D. B. Evaluation of Hydrogen Exchange Mass Spectrometry as a Stability-Indicating Method for Formulation Excipient Screening for an IgG4 Monoclonal Antibody. *J. Pharm. Sci.* **2018**, 107, 1009-1019.
(31) Wang, G. B.; Bondarenko, P. V.; Kaltashov, I. A. Multi-step conformational transitions in heat-treated protein therapeutics can be monitored in real time with temperature-controlled electrospray ionization mass spectrometry. *Analyst* **2018**, 143, 670-677.

(32) Covington, A. K.; Robinson, R. A.; Bates, R. G. The Ionization Constant of Deuterium Oxide from 5 to 50 Degrees. *J. Phys. Chem.* **1966**, 70, 3820-3824.
(33) Perrin, C. L. Proton Exchange in Amides: Surprises from Simple Systems. *Accounts of Chemical Research* **1989**, 22, 268-275.
(34) Privalov, P. L.; Khechinashvili, N. N. A Thermodynamic Approach to the Problem of Stabilization of Globular Protein Structure: A Calorimetric Study. *J. Mol. Biol.* **1974**, 86, 665-684.
(35) Coales, S. J.; E, S. Y.; Lee, J. E.; Ma, A.; Morrow, J. A.; Hamuro, Y. Expansion of time window for mass spectrometric measurement of amide hydrogen/deuterium exchange reactions. *Rapid Commun. Mass Spectrom.* **2010**, 24, 3585-3592.
(36) Goswami, D.; Devarakonda, S.; Chalmers, M. J.; Pascal, B. D.; Spiegelman, B. M.; Griffin, P. R. Time Window Expansion for HDX Analysis of an Intrinsically Disordered Protein. *J. Am. Soc. Mass Spectrom.* **2013**, 24, 1584-1592.
(37) Klinman, J. P. Dynamically Achieved Active Site Precision in Enzyme Catalysis. *Accounts Chem. Res.* **2015**, 48, 449-456.
(38) Swint, L.; Robertson, A. D. Thermodynamics of unfolding for turkey ovomucoid third domain: Thermal and chemical denaturation. *Protein Sci.* **1993**, 2, 2037-2049.
(39) Privalov, P. L.; Griko, Y. V.; Venyaminov, S. Y.; Kutyshenko, V. P. Cold Denaturation of Myoglobin. *J. Mol. Biol.* **1986**, 190, 487-498.
(40) Graziano, G. On the molecular origin of cold denaturation of globular proteins. *Phys. Chem. Chem. Phys.* **2010**, 12, 14245-14252.
(41) Yang, C.; Jang, S.; Pak, Y. A fully atomistic computer simulation study of cold denaturation of a beta-hairpin. *Nat. Commun.* **2014**, 5.
(42) Hughson, F. M.; Wright, P. E.; Baldwin, R. L. Structural Characterisation of a Partly Folded Apomyoglobin Intermediate. *Science* **1990**, 249, 1544-1548.
(43) Fändrich, M.; Fletcher, M. A.; Dobson, C. M. Amyloid fibrils from muscle myoglobin. *Nature* **2001**, 410, 165-166.
(44) Maurus, R.; Overall, C. M.; Bogumil, R.; Luo, Y.; Mauk, A. G.; Smith, M.; Brayer, G. D. A myoglobin variant with a polar substitution in a conserved hydrophobic cluster in the heme binding pocket. *Biochim. Biophys. Acta* **1997**, 1341, 1-13.
(45) Glasoe, P. K.; Long, F. A. Use of glass electrodes to measure acidities in deuterium oxide. *J. Phys. Chem.* **1960**, 64, 188-190.
(46) Reineke, K.; Mathys, A.; Knorr, D. Shift of pH-Value During Thermal Treatments in Buffer Solutions and Selected Foods. *Int. J. Food Prop.* **2011**, 14, 870-881.
(47) Kaltashov, I. A.; Bobst, C. E.; Abzalimov, R. R. H/D Exchange and Mass Spectrometry in the Studies of Protein Conformation and Dynamics: Is There a Need for a Top-Down Approach? *Anal. Chem.* **2009**, 81, 7892-7899.
(48) Dong, A. C.; Randolph, T. W.; Carpenter, J. F. Entrapping intermediates of thermal aggregation in alpha-helical proteins with low concentration of guanidine hydrochloride. *J. Biol. Chem.* **2000**, 275, 27689-27693.
(49) Bianco, V.; Alonso-Navarro, M.; Di Silvio, D.; Moya, S.; Cortajarena, A. L.; Coluzza, I. Proteins are Solitary! Pathways of Protein Folding and Aggregation in Protein Mixtures. *J. Phys. Chem. Lett.* **2019**, 10, 4800-4804.
(50) Holtzer, M. E.; Holtzer, A. Alpha-helix to random coil transitions: determination of peptide concentration from the CD at the isodichroic point. *Biopolymers* **1992**, 32, 1675-1677.
(51) Hermans, J.; Acampora, G. Reversible Denaturation of Sperm Whale Myoglobin. II. Thermodynamic Analysis. *J. Am. Chem. Soc.* **1967**, 89, 1547-1552.

(52) Smith, D. L.; Deng, Y.; Zhang, Z. Probing the Noncovalent Structure of Proteins by Amide Hydrogen Exchange Mass Spectrometry. *J. Mass Spectrom.* **1997**, 32, 135-146.
(53) Skinner, S. P.; Radou, G.; Tuma, R.; Houwing-Duistermaat, J. J.; Paci, E. Estimating Constraints for Protection Factors from HDX-MS Data. *Biophys. J.* **2019**, 116, 1194-1203.
(54) Fajer, P. G.; Bou-Assaf, G. M.; Marshall, A. G. Improved Sequence Resolution by Global Analysis of Overlapped Peptides in Hydrogen/Deuterium Exchange Mass Spectrometry. *J. Am. Soc. Mass Spectrom.* **2012**, 23, 1202-1208.
(55) Keppel, T. R.; Howard, B. A.; Weis, D. D. Mapping Unstructured Regions and Synergistic Folding in Intrinsically Disordered Proteins with Amide H/D Exchange Mass Spectrometry. *Biochemistry* **2011**, 50, 8722-8732.
(56) Nguyen, D.; Mayne, L.; Phillips, M. C.; Englander, S. W. Reference Parameters for Protein Hydrogen Exchange Rates. *J. Am. Soc. Mass Spectrom.* **2018**, 29, 1936-1939.
(57) Persson, F.; Halle, B. How amide hydrogens exchange in native proteins. *Proc. Natl. Acad. Sci. U.S.A.* **2015**, 112, 10383-10388.
(58) Best, R. B.; Vendruscolo, M. Structural interpretation of hydrogen exchange protection factors in proteins: Characterization of the native state fluctuations of CI2. *Structure* **2006**, 14, 97-106.
(59) Ratcliff, K.; Marqusee, S. Identification of Residual Structure in the Unfolded State of Ribonuclease H1 from the Moderately Thermophilic *Chlorobium tepidum*: Comparison with Thermophilic and Mesophilic Homologues. *Biochemistry* **2010**, 49, 5167-5175.
(60) Bowler, B. E. Residual structure in unfolded proteins. *Curr. Op. Struct. Biol.* **2012**, 22, 4-13.
(61) Zhu, S. L.; Shala, A.; Bezginov, A.; Sljoka, A.; Audette, G.; Wilson, D. J. Hyperphosphorylation of Intrinsically Disordered Tau Protein Induces an Amyloidogenic Shift in Its Conformational Ensemble. *PloS One* **2015**, 10, 1-15.
(62) Hamuro, Y. Determination of Equine Cytochrome c Backbone Amide Hydrogen/Deuterium Exchange Rates by Mass Spectrometry Using a Wider Time Window and Isotope Envelope. *J. Am. Soc. Mass Spectrom.* **2017**, 28, 486-497.
(63) Kan, Z. Y.; Walters, B. T.; Mayne, L.; Englander, S. W. Protein hydrogen exchange at residue resolution by proteolytic fragmentation mass spectrometry analysis. *Proc. Natl. Acad. Sci. U.S.A.* **2013**, 110, 16438-16443.
(64) Gessner, C.; Steinchen, W.; Bedard, S.; Skinner, J. J.; Woods, V. L.; Walsh, T. J.; Bange, G.; Pantazatos, D. P. Computational method allowing Hydrogen-Deuterium Exchange Mass Spectrometry at single amide Resolution. *Sci. Rep.* **2017**, 7.
(65) Ascolese, E.; Graziano, G. On the cold denaturation of globular proteins. *Chem. Phys. Lett.* **2008**, 467, 150-153.
(66) Dias, C. L.; Ala-Nissila, T.; Karttunen, M.; Vattulainen, I.; Grant, M. Microscopic mechanism for cold denaturation. *Phys. Rev. Lett.* **2008**, 100, 118101.

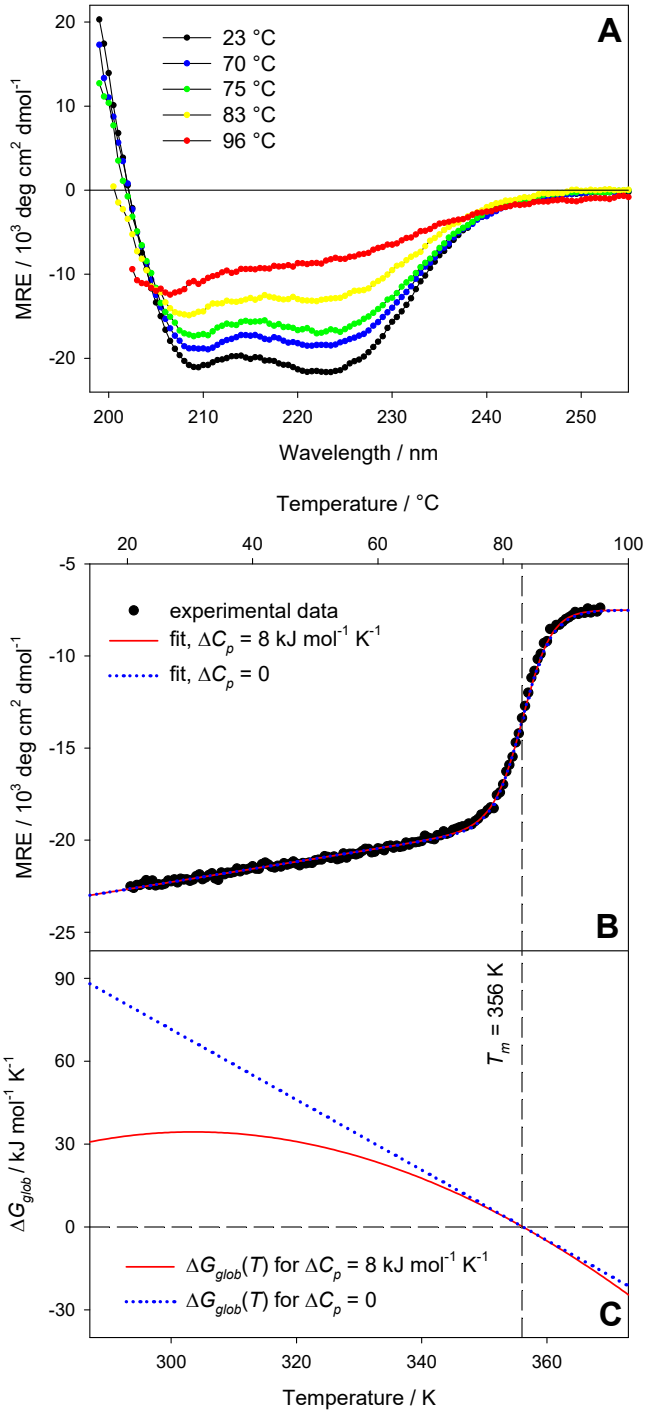

FIGURE 1. Thermal unfolding of 5 μM Mb studied by CD spectroscopy. (A) CD spectra acquired at various temperatures, displaying mean residue ellipticity (MRE) vs. wavelength. (B) Unfolding profile monitored at 222 nm, heating rate 1 °C min^{-1}. Black symbols are experimental data, colored lines represent fits for two different values of ΔC_p. (C) Free energy $\Delta G_{glob}(T)$ of the N ↔ U equilibrium according to eqs. 3 and 4; parameters were extracted from the fits of panel B.

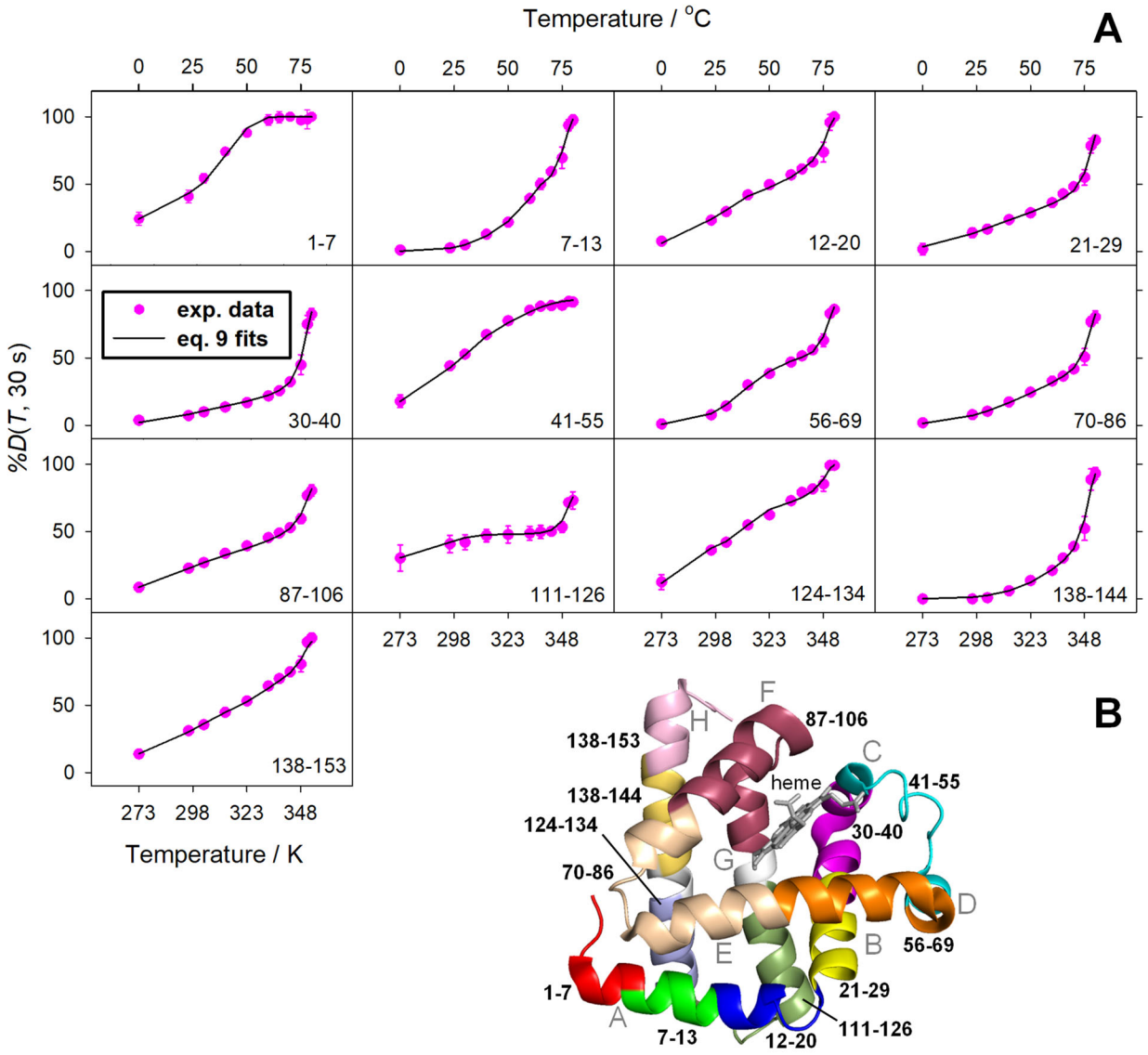

FIGURE 2. (A) Deuteration percentage *%D* as a function of temperature *T* for a labeling time of *t* = 30 s. The sequence range of each peptide is indicated. Pink symbols represent experimental data, black lines are fits based on eq. 9. (B) Locations of panel A peptides in the Mb crystal structure. The cartoon also highlights the eight α-helices A-H.

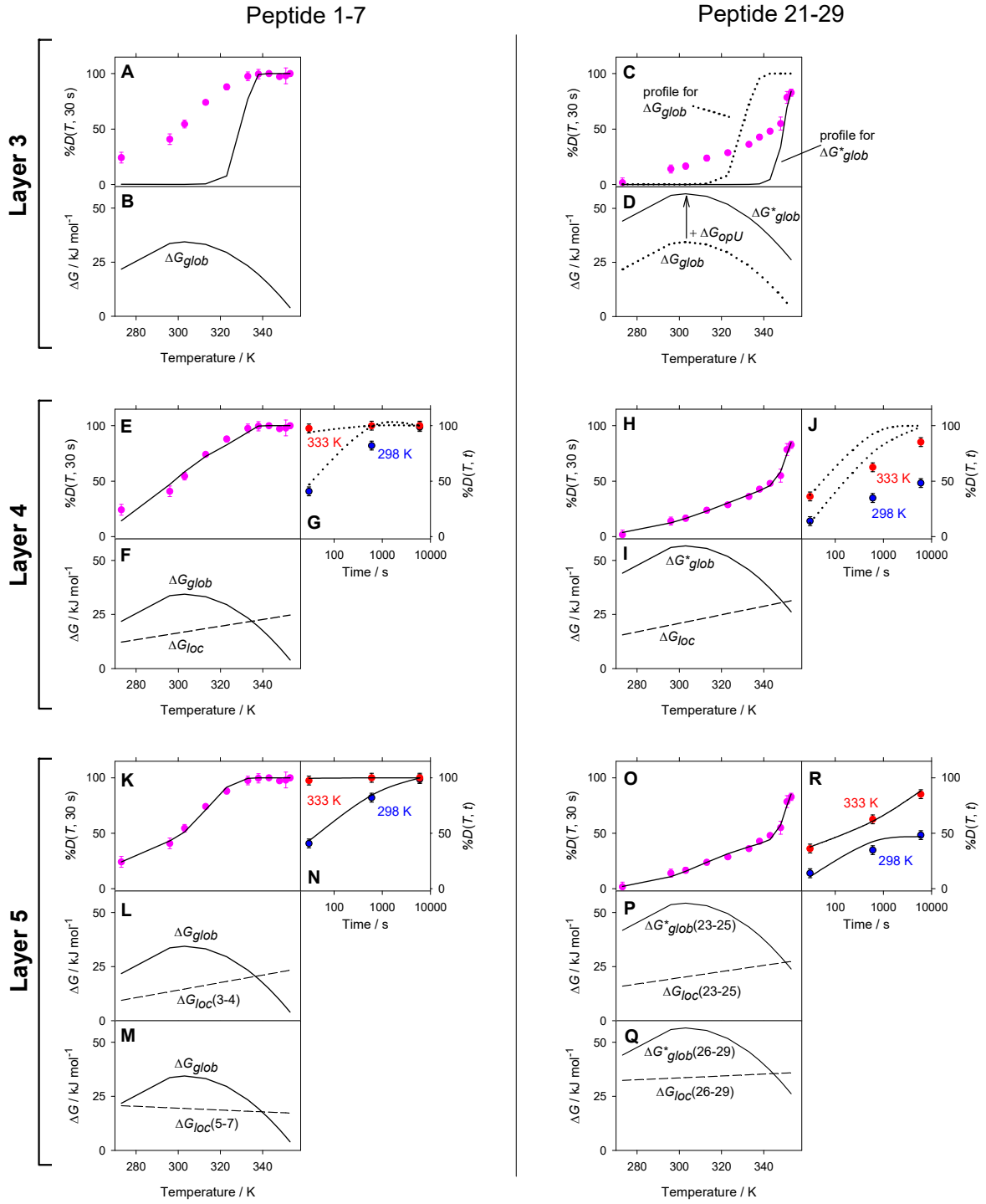

FIGURE 3. Layer-by-layer development of a model for interpreting HDX-MS data recorded as a function of temperature T and labeling time t. Circles represent experimental $\%D(T, t)$ data for peptides 1-7 and 21-29. Note how the quality of the fits improves for A → K/N and C → O/R. For Layers 1and 2, see text. Layer 3: Global dynamics with and without ΔG_{opU}. Layer 4: Inclusion of simple local dynamics. Layer 5: Inclusion of local dynamics where each peptide was dissected into two segments that undergo independent opening/closing. Layer 5 parameters for Peptide 1-7: ΔG_{opU}(3-4) = 0, ΔH_{loc}(3-4) = -38, ΔS_{loc}(3-4) = -174, ΔG_{opU}(5-7) = 0, ΔH_{loc}(5-7) = 33, ΔS_{loc}(5-7) = 43. For Peptide 21-29: ΔG_{opU}(23-25) = 20, ΔH_{loc}(23-25) = -23, ΔS_{loc}(23-25) = -143, ΔG_{opU}(26-29) = 22, ΔH_{loc}(26-29) = 20, ΔS_{loc}(26-29) = -44 (ΔG_{opU} and ΔH_{loc} in kJ mol^{-1}; ΔS_{loc} in J mol^{-1} K^{-1}).

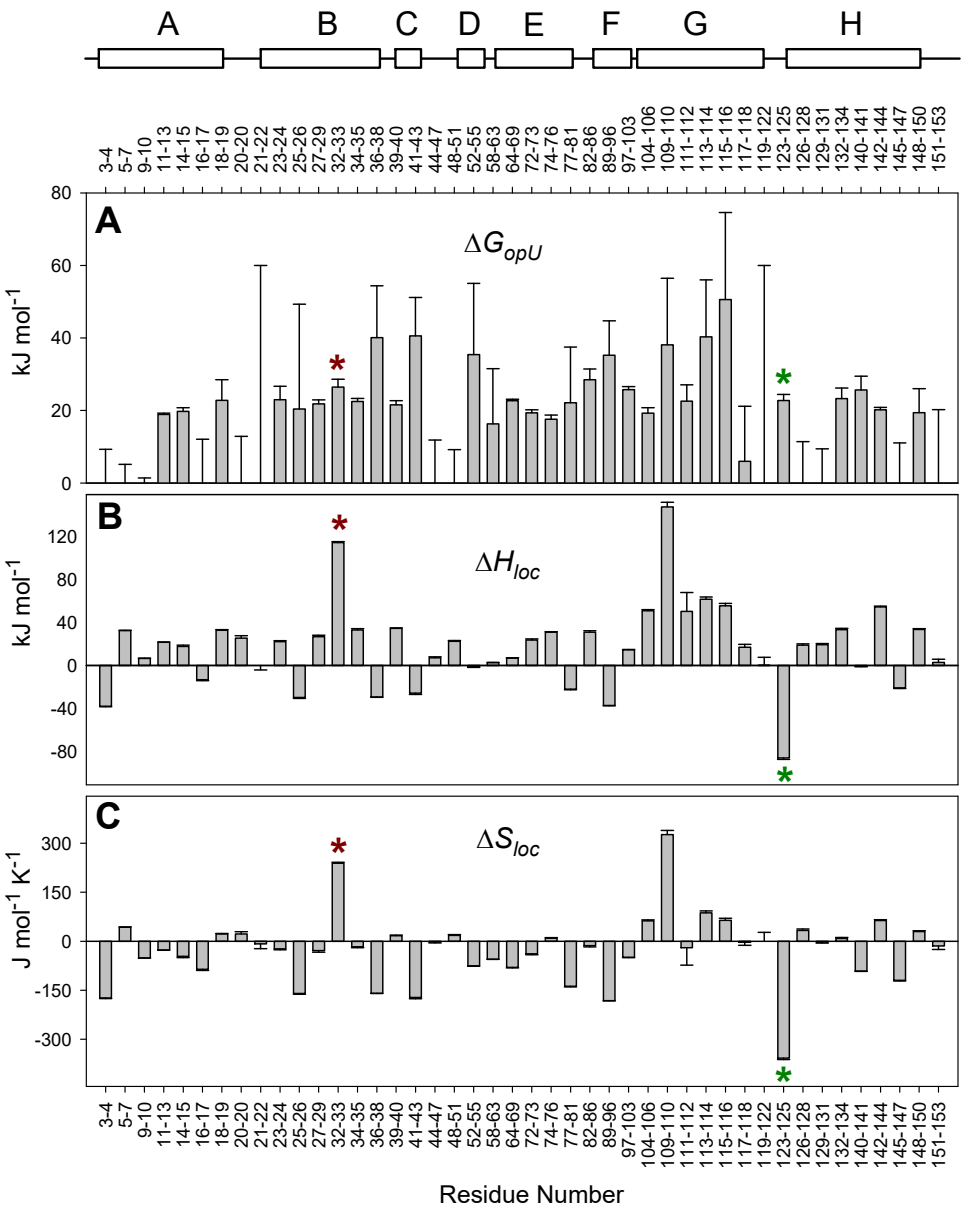

FIGURE 4. ΔG_{opU}, ΔH_{loc}, and ΔS_{loc} determined by global fitting of temperature- and time-dependent HDX-MS data for 44 segments along the Mb sequence. Shown at the top is the Mb secondary structure with helices A-H. Plots of $\Delta G_{glob}^{*}(T)$ and $\Delta G_{loc}(T)$ derived from the parameters shown here are summarized in Figure S8. Errors bars indicate by how much each value could be altered to cause a 10% increase of X^2. Asterisks highlight two segments that are further examined in Figure 5.

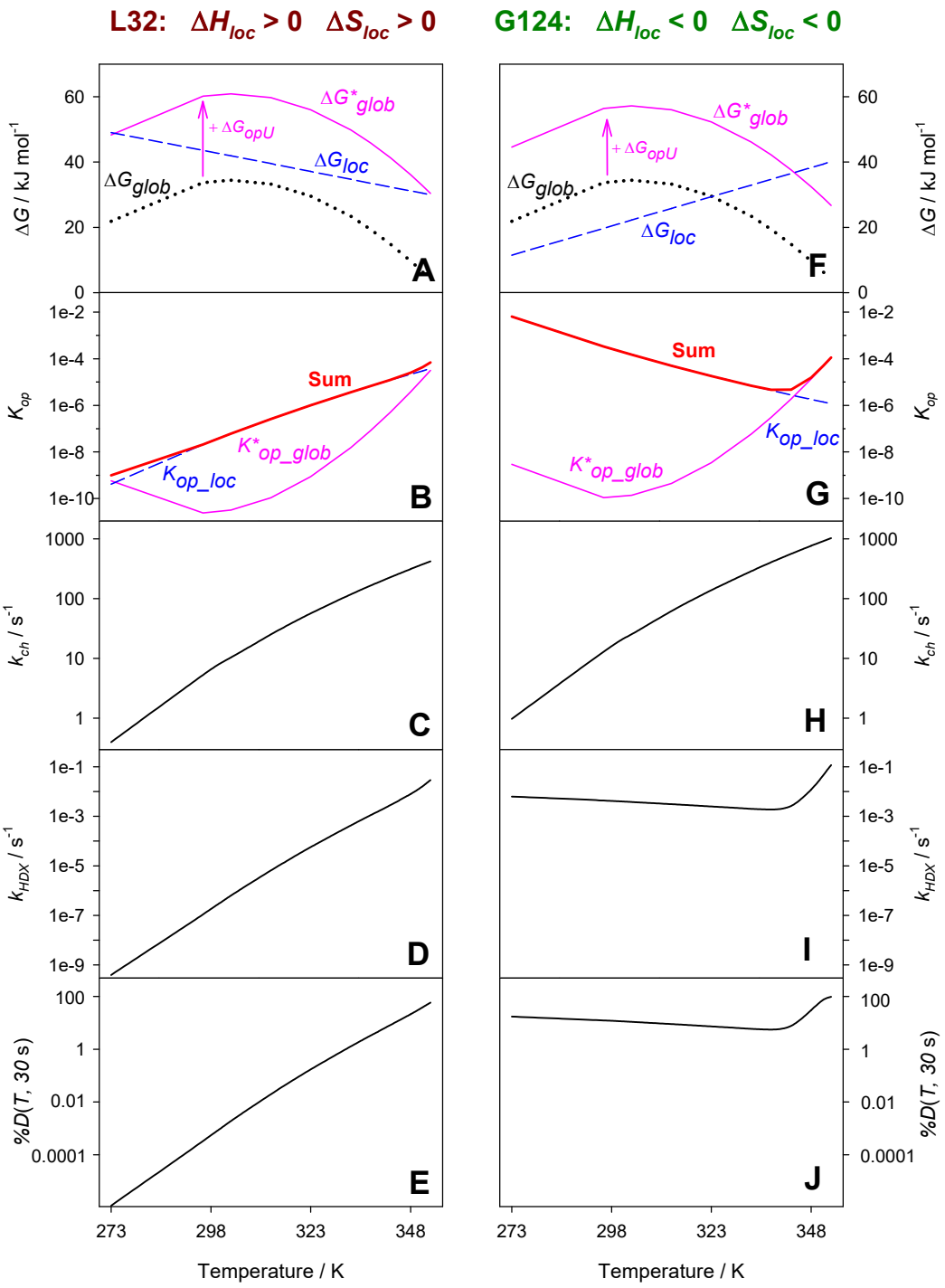

FIGURE 5. Temperature-dependent HDX events, illustrated for the backbone NH sites of L32 (left) and G124 (right). (A, F) Free energy profiles for local and global fluctuations, calculated from ΔG_{opU}, ΔH_{loc}, and ΔS_{loc} parameters of Figure 4. (B, G) Conversion of free energy to equilibrium constants, along with their sum (red lines, eq. 8). (C, H) $k_{ch,32}$ and $k_{ch,124}$, calculated using eq. 6b. (D, I) $k_{HDX,32}$ and $k_{HDX,124}$, calculated as the product of "Sum" in panels B/G, and k_{ch} in panels C/H (eq. 8). (E, J) *%D* for a labeling time of 30 s. Note that except for A/F, all panels have logarithmic *y*-axes.

FOR TOC ONLY

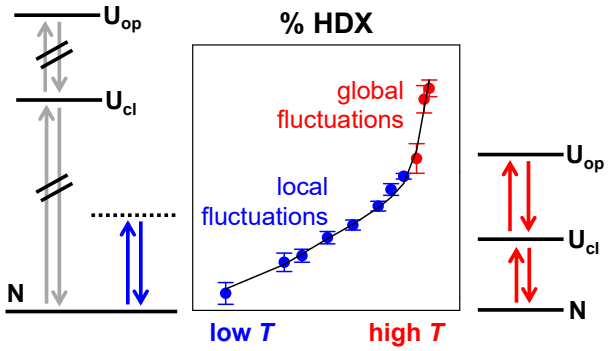
U_{op}
U_{cl}
N
% HDX
global
fluctuations
local
fluctuations
low *T*
high *T*
U_{op}
U_{cl}
N